PALEOCEANOGRAPHY, VOL. 28, 91–104, doi:10.1002/palo.20014, 2013

# Deglacial development of (sub) sea surface temperature and salinity in the subarctic northwest Pacific: Implications for upper-ocean stratification

Jan-Rainer Riethdorf,[1,3] Lars Max,[2] Dirk Nürnberg,[1] Lester Lembke-Jene,[2] and Ralf Tiedemann[2]

Received 25 June 2012; revised 13 January 2013; accepted 17 January 2013; published 23 March 2013.

[1] Based on models and proxy data, it has been proposed that salinity-driven stratification weakened in the subarctic North Pacific during the last deglaciation, which potentially contributed to the deglacial rise in atmospheric carbon dioxide. We present high-resolution subsurface temperature ($T_{Mg/Ca}$) and subsurface salinity-approximating ($\delta^{18}O_{ivc\text{-}sw}$) records across the last 20,000 years from the subarctic North Pacific and its marginal seas, derived from combined stable oxygen isotopes and Mg/Ca ratios of the planktonic foraminiferal species *Neogloboquadrina pachyderma* (sin.). Our results indicate regionally differing changes of subsurface conditions. During the Heinrich Stadial 1 and the Younger Dryas cold phases, our sites were subject to reduced thermal stratification, brine rejection due to sea-ice formation, and increased advection of low-salinity water from the Alaskan Stream. In contrast, the Bølling-Allerød warm phase was characterized by strengthened thermal stratification, stronger sea-ice melting, and influence of surface waters that were less diluted by the Alaskan Stream. From direct comparison with alkenone-based sea surface temperature estimates ($SST_{Uk'37}$), we suggest deglacial thermocline changes that were closely related to changes in seasonal contrasts and stratification of the mixed layer. The modern upper-ocean conditions seem to have developed only since the early Holocene.

**Citation:** Riethdorf, J.-R., L. Max, D. Nürnberg, L. Lembke-Jene, and R. Tiedemann (2013), Deglacial development of (sub) sea surface temperature and salinity in the subarctic northwest Pacific: Implications for upper-ocean stratification, *Paleoceanography*, *28*, 91–104, doi:10.1002/palo.20014.

## 1. Introduction

[2] No deep water is formed in the modern subarctic North Pacific (N Pacific). There, a relatively steep salinity gradient (permanent halocline) prevents surface water from sinking, isolating it from the underlying nutrient-rich deep water [*Haug et al*., 1999]. In the N Pacific, upper-ocean stratification most likely developed around 2.7 million years ago [*Haug et al*., 1999, 2005; *Sigman et al*., 2004] and is maintained by a restricted meridional exchange between subpolar and subtropical waters, atmospheric low-latitude moisture transport from the Atlantic to the Pacific, and northward moisture flux by the Asian monsoon [*Warren*, 1983; *Emile-Geay et al*., 2003]. As a consequence of salinity-driven stratification, the exchange of gas, heat, and nutrients between deep and surface water is limited in the N Pacific. In contrast, the modern Southern Ocean releases carbon dioxide ($CO_2$) to the atmosphere due to upwelling of deep waters. This led to the assumption that high-latitude ocean stratification drives changes in atmospheric $CO_2$ concentrations during recent glacial-interglacial cycles [*Haug et al*., 1999; *Sigman and Boyle*, 2000; *Sigman and Haug*, 2003; *Sigman et al*., 2004, 2010; *Jaccard et al*., 2005]. However, growing paleoceanographic evidence [e.g., *Okazaki et al*., 2010] indicates that during the last deglaciation, deep water was formed in the N Pacific and that the regional halocline was not a permanent feature. Hence, the N Pacific might have contributed to the deglacial rise of atmospheric $CO_2$.

[3] High-resolution records depicting the deglacial paleoceanographic evolution in the subarctic N Pacific are sparse due to a shallow lysocline and corrosive bottom waters limiting $CaCO_3$ preservation. Available reconstructions of sea surface temperature (SST) and salinity indicate strong oceanographic changes and climate oscillations in the subarctic N Pacific realm during the last deglaciation (20–10 ka BP) [e.g., *Ternois et al*., 2000; *Sarnthein et al*., 2004, 2006; *Gebhardt et al*., 2008; *Sagawa and Ikehara*, 2008; *Caissie et al*., 2010], which are similar to those recorded in Greenland ice [*Grootes et al*., 1993; *NGRIP members*, 2004]. These are the cold periods of the Heinrich Stadial 1

Additional supporting information may be found in the online version of this article.

[1]Helmholtz Centre for Ocean Research Kiel (GEOMAR), Kiel, Germany.
[2]Alfred Wegener Institute for Polar and Marine Research, Bremerhaven, Germany.
[3]Department of Ocean Floor Geoscience, Atmosphere and Ocean Research Institute, University of Tokyo, Kashiwa, Chiba, Japan.

Corresponding author: Jan-Rainer Riethdorf, Helmholtz Centre for Ocean Research Kiel (GEOMAR), Wischhofstr. 1-3, D-24148 Kiel, Germany. (jriethdorf@geomar.de)


0883-8305/13/10.1002/palo.20014

(H1, 18.0–14.7 ka BP) [*Sarnthein et al*., 2001] and the Younger Dryas (YD, ~12.9–11.7 ka BP) [*Blockley et al*., 2012], and the warm phases of the Bølling-Allerød (B/A, ~14.7–12.9 ka BP) [*Blockley et al*., 2012] and the Preboreal (PB, ~11.7–11.0 ka BP). Recent studies also found evidence for deep water ventilation in the NW Pacific during H1 and the YD [*Ahagon et al*., 2003; *Ohkushi et al*., 2004; *Sagawa and Ikehara*, 2008; *Okazaki et al*., 2010], while at the same time the Atlantic meridional overturning circulation (AMOC) collapsed or declined [*McManus et al*., 2004]. In contrast, during the B/A, higher ventilation ages have been found in the western N Pacific, which is indicative of reduced deep water ventilation [*Okazaki et al*., 2010]. In agreement with this observation, general circulation models predict a strengthening of the Pacific meridional overturning circulation (PMOC), which results from a rise in salinity in the N Pacific due to a weakened AMOC [e.g., *Menviel et al*., 2012]. These studies controversially argue either for an atmosphere-controlled "in-phase" [*Mikolajewicz et al*., 1997; *Krebs and Timmermann*, 2007; *Okumura et al*., 2009] or for an ocean-controlled "antiphase" [*Schmittner et al*., 2003, 2007; *Saenko et al*., 2004] relationship between the thermal evolution of the North Atlantic (N Atlantic) and the N Pacific. The antiphase relationship is supported by SST and salinity reconstructions from planktonic foraminifera at Site MD01-2416 and ODP Site 883 indicating that during H1, maxima in SST were accompanied by increased salinity [*Kiefer et al*., 2001; *Sarnthein et al*., 2006; *Gebhardt et al*., 2008]. Higher salinity during H1 is supported by Mg/Ca- and $\delta^{18}O$-based results from core GH02-1030 off Japan [*Sagawa and Ikehara*, 2008], which also argues for a potential disappearance of the halocline. The results from core MD01-2416, however, are in conflict with alkenone-based SST reconstructions from the N Pacific realm, which are more supportive of the in-phase models. Results indicate restricted marine productivity during H1 and a SST maximum that occurred during the subsequent B/A in the NE Pacific [*Kienast and McKay*, 2001; *Barron et al*., 2003], the Bering Sea [*Caissie et al*., 2010; *Max et al*., 2012], and the Okhotsk Sea [*Ternois et al*., 2000; *Harada et al*., 2006a; *Seki et al*., 2009]. Mg/Ca-based results from core GH02-1030 also show a rise in SST during the B/A [*Sagawa and Ikehara*, 2008]. In summary, these observations may point to a regionally differing development of the thermocline, because sites MD01-2416 (Detroit Seamount, open subarctic NW Pacific) and GH02-1030 (Kuroshio-influenced NW Pacific) provide quite different oceanographic settings with respect to the N Pacific marginal seas. Consequently, additional reconstructions of SST and salinity, which allow for direct comparisons between alkenone- and Mg/Ca-based results, are essential to understand changes in the structure of the upper water column and the SST development of the subarctic N Pacific.

[4] Here, we report combined stable oxygen isotope and Mg/Ca-based reconstructions of subsurface temperatures ($T_{Mg/Ca}$) and $\delta^{18}O_{ivc\text{-}sw}$ (approximating subsurface salinity) from sediment cores recovered from the southern Okhotsk Sea, the NW Pacific off Kamchatka, and the western Bering Sea covering the last 20 ka BP. Our results, which are compared to alkenone-based SST estimates ($SST_{Uk'37}$) derived from the same samples [*Max et al*., 2012], indicate deglacial variations in mixed layer stratification (MLS). Moreover, we present supporting evidence that the modern salinity-driven stratification in the N Pacific is a relatively recent feature as suggested by *Sarnthein et al*. [2004].

## 2. Regional Setting

[5] The subarctic N Pacific is characterized by a large-scale cyclonic surface circulation pattern (Figure 1). At ~40°N, the North Pacific Current, an extension of the subtropical Kuroshio Current, flows eastward and brings relatively warm water (~10°C) into the Alaskan gyre in the NE Pacific. From here, the Alaskan Current, fed by freshwater discharge from the North American continent [*Kowalik et al*., 1994; *Weingartner et al*., 2005], transports surface water to the north. Subsequently, the Alaskan Stream flows westward along the Aleutian Island Arc, thereby causing surface water to flow into the Bering Sea through several passes. Within the Bering Sea, a cyclonic surface circulation develops with the East Kamchatka Current (EKC) and the Bering Slope Current acting as boundary currents. Cold and nutrient-rich surface waters leave the Bering Sea through Bering Strait into the Arctic Ocean, but the main outflow occurs back into the NW Pacific via Kamchatka Strait [e.g., *Stabeno et al*., 1999]. The northern straits of the Kurile Islands provide inflow of Pacific water from the EKC into the Okhotsk Sea [e.g., *Katsumata and Yasuda*, 2010]. In the Okhotsk Sea, the surface circulation pattern is also cyclonic. Notably, brine rejection due to sea-ice formation leads to the production of Okhotsk Sea intermediate water (OSIW), which determines the potential density ($\sigma_0$) surface of NPIW in the N Pacific. OSIW flows out of the Okhotsk Sea through the Kurile Straits, thereby mixing with waters from the Western Subarctic Gyre [*Yasuda*, 1997; *You*, 2003]. The Oyashio Current transports this relatively cold (~4°C), low-salinity (~33 psu) water along the Kurile Islands to the east of Japan, where it meets with warmer and saltier water (~34–35 psu) from the Kuroshio. Cabbeling of these water masses then forms NPIW.

[6] Characteristic oceanographic features of the subarctic NW Pacific are the strong seasonal variability of SST and the marked upper-ocean stratification due to the buoyant low-salinity surface layer (Figure 2). Both are linked to the seasonal interplay between the Siberian High and the Aleutian Low, which in the Okhotsk and Bering seas leads to intense winter mixing and to seasonal sea-ice formation [e.g., *Niebauer et al*., 1999]. Especially during winter, the sea-ice cover is significantly expanded in both marginal seas and in the vicinity of the eastern Kamchatka continental margin. Sea-ice formation releases brines, which sink in the water column resulting in increased subsurface salinity. During summer, MLS arises from increased insolation and melting sea-ice, while a temperature minimum layer (dichothermal layer) remains at ca. 100 m (Figure 2). Waters from this layer are believed to be formed during winter in the Bering and Okhotsk seas and to be subsequently exported to the NW Pacific [*Ohtani et al*., 1972; *Miura et al*., 2002]. At our study sites, the modern seasonal thermo- and pycnoclines lie within 0–100 m. The permanent halocline lies deeper (~100–200 m), and it further deepens toward the northern part of the Bering Sea, as do the mixed and the dichothermal layers (Figure 2). Notably, the calcite saturation horizon (CSH) at our sites lies between 150 and

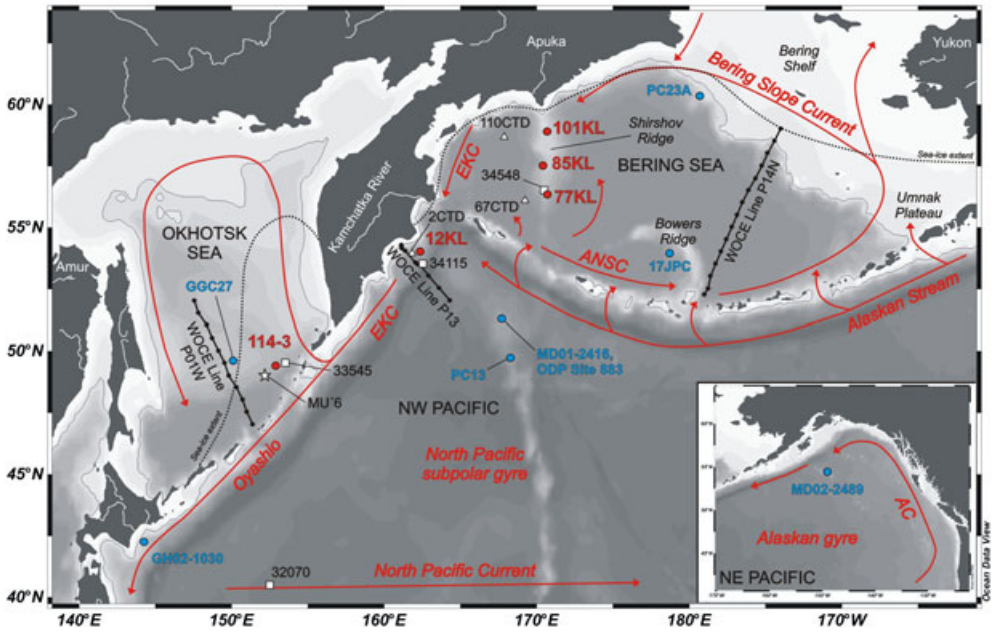


**Figure 1.** Bathymetric map with 250 m isobathe of the subarctic NW Pacific, Okhotsk Sea, Bering Sea, and NE Pacific (inlet). Red dots indicate sediment cores studied here, blue dots denote published reference records: MD01-2416 and ODP Site 883 [*Sarnthein et al*., 2004, 2006; *Gebhardt et al*., 2008], and PC13 [*Brunelle et al*., 2010] from the NW Pacific, MD02-2489 from the NE Pacific [*Gebhardt et al*., 2008], GH02-1030 off Japan [*Sagawa and Ikehara*, 2008], GGC27 from the Okhotsk Sea [*Brunelle et al*., 2010], HLY-02-02-17JPC from Bowers Ridge [*Brunelle et al*., 2007, 2010], and MR06-04-PC23A from the upper slope of the NE Bering Sea [*Rella et al*., 2012]. CTD stations from R/V Sonne expedition SO201-2 (white triangles) [*Dullo et al*., 2009], WOA 2009 stations (white squares) [*Locarnini et al*., 2010], and stations from the World Ocean Circulation Experiment (WOCE; black dots) referred to in the text are included. The white star marks the position of Okhotsk Sea station MU'6 [*Yamamoto et al*., 2001]. The general surface circulation pattern [after *Tomczak and Godfrey*, 1994; *Stabeno et al*., 1999] is indicated by red arrows, and the dotted line marks the modern average winter sea-ice extent (after *Niebauer et al*., 1999; *IRI/LDEO Climate Data Library*, http://iridl.ldeo.columbia.edu/). AC = Alaskan Current, EKC = East Kamchatka Current, ANSC = Aleutian North Slope Current. This map was generated with "Ocean Data View" [*Schlitzer*, 2011].

300 m, which has implications for our carbonate-based proxy reconstructions (Supplementary Information).

## 3. Material and Methods

### 3.1. Sedimentology and Age Models

[7] This study is based on piston cores SO201-2-12KL, -77KL, -85KL, and -101KL recovered during R/V Sonne cruise SO201 KALMAR Leg 2 in the NW Pacific off Kamchatka and in the western Bering Sea [*Dullo et al*., 2009] (Table 1). Sediments are dominated by siliciclastic material of mainly clay and silt size, which are intercalated by thin layers of diatomaceous ooze/silt. Additional samples stem from core LV29-114-3 retrieved from the southern Okhotsk Sea during cruise LV29 KOMEX Leg 2 with R/V Akademik Lavrentyev [*Biebow et al*., 2003] (Table 1). In this core, terrigenous sediments are overlain on top by a 175 cm thick layer of diatomaceous sediment. Sites 12KL and 114-3 are influenced by the EKC. All cores contain low contents of $CaCO_3$ (<5 wt %). However, all cores show increased $CaCO_3$ contents of up to 30 wt % during the B/A.

[8] Age models are based on a combined chronostratigraphic approach including high-resolution spectrophotometric (color b*) and X-ray fluorescence (XRF) core logging data for intercore correlations, as well as accelerator mass spectrometry (AMS) radiocarbon dating of planktonic foraminifera. The stratigraphic framework of all cores including the AMS-$^{14}$C dating results is presented in detail in *Max et al*. [2012] and in the Supplementary Information.

### 3.2. Stable Isotope and Mg/Ca Analyses

[9] Combined stable oxygen isotope ($\delta^{18}O$) and Mg/Ca analyses were performed on ~500 µg (~100–150 tests) of the polar to subpolar subsurface–dwelling planktonic foraminifer *Neogloboquadrina pachyderma* (sin.) (referred to as *Nps* hereafter), selected from the 125–250 µm size fraction. We focused on the most abundant four-chambered specimen of *Nps*. Abundance of foraminiferal tests was sufficient in all sediment cores, except for core 12KL, which lacked sufficient amounts after 6 ka BP. $\delta^{18}O$ was measured using a MAT 253 mass spectrometer (Thermo Scientific, Germany) coupled with a Kiel IV Carbonate device (Thermo Scientific, Germany). Results were calibrated to the VPDB scale and referenced to the NBS19 standard. Analytical long-term precision ($n > 1000$ samples) of the used in-house carbonate standard (Solnhofen limestone) was

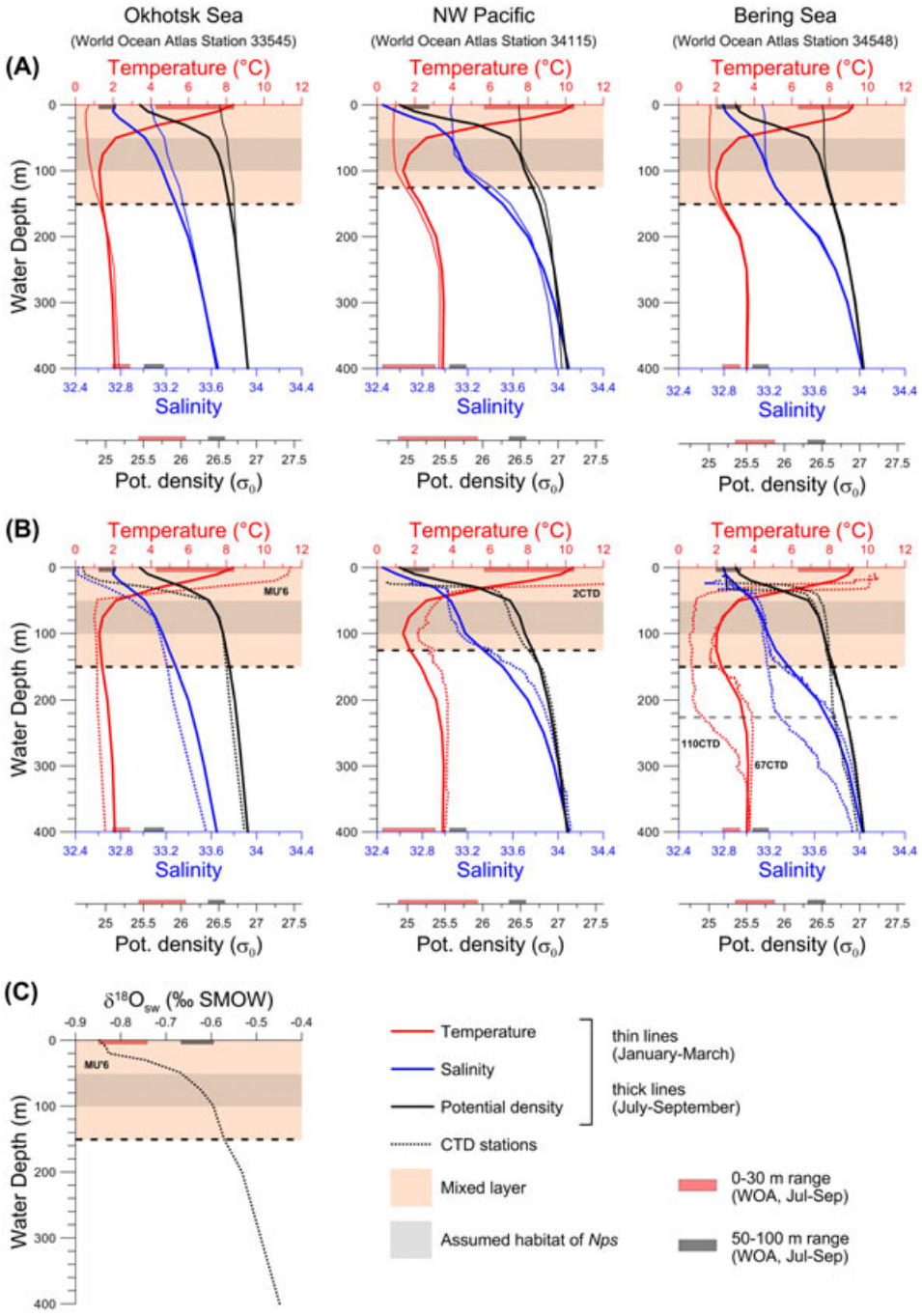


**Figure 2.** (A, B) Modern seasonal profiles of in situ temperature, salinity, and potential density ($\sigma_0$) during boreal winter (January-March, thin lines) and summer (July-September, thick lines), as well as actual seawater $\delta^{18}O_{sw}$ data (C) for the southern Okhotsk Sea, the subarctic NW Pacific, and the western Bering Sea. Stations were chosen from WOA 2009 (stations 33545, 34115, 34548) [*Locarnini et al*., 2010] (cf. Figure 1). In (B), summer conditions are shown together with CTD data of R/V Sonne expedition SO201-2 from September 2009 (stations SO201-2-2CTD, -67CTD, -110CTD) [*Dullo et al*., 2009]. $\delta^{18}O_{sw}$ data from Okhotsk Sea station MU'6 are from *Yamamoto et al*. [2001]. The habitat of the planktonic foraminifer *N. pachyderma* (sin.) is assumed to lie in 50–100 m (gray-shaded areas) and to be associated with an isopycnal layer. The modern hydrographic ranges of the photic zone (0–30 m) and of the subsurface in 50–100 m are represented by red and gray bars, respectively, next to the abscissae. Maximum mixed layer depths (dashed line) are inferred from *Miura et al*. [2002] and fit WOA and CTD data. Note the thicker mixed and dichothermal layer at Bering Sea station 110CTD.

**Table 1.** Site Information

| Core | Latitude | Longitude | Depth (mbsl) | Recovery (m) |
|---|---|---|---|---|
| LV29-114-3 | 49°22.54'N | 152°53.23'E | 1765 | 9.64 |
| SO201-2-12KL | 53°59.47'N | 162°22.51'E | 2145 | 9.05 |
| SO201-2-77KL | 56°19.83'N | 170°41.98'E | 2135 | 11.78 |
| SO201-2-85KL | 57°30.30'N | 170°24.77'E | 968 | 18.13 |
| SO201-2-101KL | 58°52.52'N | 170°41.45'E | 630 | 18.32 |

±0.06‰. Cleaning of foraminiferal tests for Mg/Ca analyses followed the protocol of *Barker et al*. [2003] and included an additional reductive cleaning step. Samples were measured on an axial viewing ICP-OES (VARIAN 720-ES) with an analytical long-term precision of ±0.1 mmol mol$^{-1}$ for Mg/Ca of the ECRM752-1 standard. For core 114-3, earlier measurements were included in our data set to improve sampling resolution. These measurements used 30 specimens of *Nps* (150–250 μm size fraction) to determine $\delta^{18}O$ and 50 specimens for Mg/Ca analyses. Cleaning also followed the protocol of *Barker et al*. [2003], but did not include reductive cleaning. A radially viewing ICP-OES (Ciros CCD SOP, Spectro A.I.) was used to determine Mg/Ca. Method details are given in the Supplementary Information.

### 3.3. Mg/Ca Temperature Signal of *Nps*

[10] As there is no locally established temperature-Mg/Ca calibration for *Nps* in the subarctic N Pacific, we applied the linear equation of *Kozdon et al*. [2009]. It is based on Holocene core-top samples from high-latitude Nordic Seas used in a cross-calibration approach between Mg/Ca and independent $\delta^{44/40}Ca$ measurements.

$$\mathrm{Mg/Ca}\left(\mathrm{mmol\ mol^{-1}}\right) = 0.13\mathrm{Temp.}(^{\circ}\mathrm{C}) + 0.35 \qquad (1)$$

[11] Considering the slope in equation (1), the analytical precision for Mg/Ca translates into an uncertainty of ±0.8°C. Results of *Kozdon et al*. [2009] indicated variable calcification depths of *Nps* that are associated with an isopycnal layer. Most other temperature calibrations for *Nps* are of exponential character and assume constant calcification depths. We consider the habitat of N Pacific *Nps* likely to be related to the seasonal thermo- and pycnoclines, similar to the Nordic Seas and the Arctic Ocean. Other studies conducted there showed that shell calcification of *Nps* mostly occurs at or close to the thermocline in 50–200 m [*Kohfeld et al*., 1996; *Bauch et al*., 1997; *Simstich et al*., 2003]. Based on these studies, *Sarnthein et al*. [2004, 2006] assumed a depth range of 30–100 m in the NW Pacific. For the Okhotsk Sea, *Bauch et al*. [2002] suggested average calcification depths at 50–200 m and concluded that *Nps* lives at the bottom of the thermocline. Tow samples from the NW Pacific showed that the habitat of *Nps* lies below the pycnocline (>20 m) [*Kuroyanagi and Kawahata*, 2004]. Accordingly, we assume that the habitat of *Nps* lies at 50–100 m at our sites. Considering data from the World Ocean Atlas (WOA), this depth range lies below the summer (July-September) pycnocline, extends to the bottom of the summer thermocline, and is associated with an isopycnal layer ($\sigma_0 \approx 26.4\ \mathrm{kg\,m^{-3}}$; Figure 2). Additional support for the assumption of calcification at subsurface levels comes from the comparison of the foraminiferal $\delta^{18}O$ signal to what would be predicted for the $\delta^{18}O$ signal of seawater ($\delta^{18}O_{sw}$) when using the hydrographic temperature data (Supplementary Information).

[12] It has been suggested that in the NW Pacific, *Nps* represents late spring and late summer/early fall temperatures [*Sarnthein et al*., 2006; *Gebhardt et al*., 2008], which is supported by sediment trap studies [*Takahashi et al*., 2002; *Kuroyanagi et al*., 2012]. Results for the southern Bering Sea and the NW Pacific Subarctic Front reveal that the main peak in $CaCO_3$ depositional flux occurs during late summer/early fall [*Takahashi et al*., 2002; *Mohiuddin et al*., 2005]. We therefore assume that at our study sites, which are additionally influenced by winter sea-ice, the main Mg/Ca signal of *Nps* likely represents late summer/early fall. This is supported by our reconstructed average Holocene (<8 ka BP) $T_{Mg/Ca}$ estimates of 3–4°C, which is only 1–2°C warmer than during modern summer and fall at 50–100 m. In contrast, modern winter (January-March) and spring temperatures lie below 3°C in 0–100 m (Figure 2).

[13] Our Mg/Ca results might be partly influenced by dissolution of the foraminiferal tests in conjunction with selective removal of $Mg^{2+}$ ions [e.g., *Regenberg et al*., 2006, and references therein], especially since our sediment cores were recovered below the modern CSH. Variations in Mg/Ca might thus be related to changes in $CaCO_3$ preservation. However, we refrained from correcting the initial Mg/Ca values as clear relationships between $CaCO_3$ contents and foraminiferal Mg/Ca were not found and correction procedures for contamination/dissolution effects were considered unsuitable (Supplementary Information).

### 3.4. Combined Use of Mg/Ca- and Alkenone-Based Temperatures

[14] We compared our $T_{Mg/Ca}$ records with the $SST_{Uk'37}$ records of *Max et al*. [2012], which were derived from the same samples. *Max et al*. [2012] used the calibration of *Müller et al*. [1998], which is widely used in N Pacific SST reconstructions providing a standard error of ±1.5°C. For the NW Pacific and both marginal seas, it has been shown that alkenones are mainly synthesized by *Emiliania huxleyi* during late summer to early fall within the upper 50 m [*Harada et al*., 2003, 2006b; *Seki et al*., 2007]. At our sites, surface sediment $SST_{Uk'37}$ of 5–7°C (not shown) falls within 1–2°C when compared with the modern instrumental range at 0–50 m (Figure 2).

[15] Differences between $SST_{Uk'37}$ and $T_{Mg/Ca}$ can result from seasonal bias [e.g., *Leduc et al*., 2010]. However, for our sites we assume a restriction of both, coccolithophores and planktonic foraminifera, to the sea-ice-free late summer/early fall season. Nevertheless, we consider that a seasonal bias might have influenced the proxy records under conditions of reduced regional sea-ice influence, e.g., during the B/A. Accordingly, a high temperature gradient ($\Delta T$) between $SST_{Uk'37}$ and $T_{Mg/Ca}$ is thought to reflect enhanced thermal MLS. However, the combined uncertainty for $SST_{Uk'37}$ and $T_{Mg/Ca}$ is substantial (±2.3°C), and significant temporal trends in the records are needed for interpretation of $\Delta T$. In addition, $\Delta T$ might be influenced by intensified insolation as well as by variations in the exchange of heat between the upper and the deep ocean [*Kohfeld et al*., 1996; *Andersson et al*., 2010].

### 3.5. Ice Volume–Corrected $\delta^{18}O_{sw}$ and the Influence of Brines

[16] We used ice volume–corrected estimates of the local seawater oxygen isotopic composition ($\delta^{18}O_{ivc\text{-}sw}$; reported in ‰ versus SMOW) to approximate past changes in local salinity. $\delta^{18}O_{sw}$ was calculated by applying the relationship of *Shackleton* [1974]. Finally, we corrected for the global ice-volume signal following *Waelbroeck et al*. [2002]. The conversion of $\delta^{18}O_{sw}$ into salinity relies on regional calibrations. Such calibrations exist for the Okhotsk Sea and the western subarctic Pacific [*Yamamoto et al*., 2001, 2002]. However, the uncertainty of the $\delta^{18}O_{sw}$ approach (~0.3‰) already translates into a salinity error of ca. ±0.8 when applying the calibration of *Yamamoto et al*. [2001]. Since our study sites show seasonal salinity variations of ~0.4–0.7 at 0–100 m (Figure 2), we did not apply a respective conversion. A shift in $\delta^{18}O_{ivc\text{-}sw}$ toward more positive values, hence, is thought to reflect a rise in local salinity, and vice versa.

[17] In the high latitudes, the salinity-$\delta^{18}O_{sw}$ relationship is not linear due to sea-ice-related brine rejection [e.g., *Bauch et al*., 1995, 1997; *Yamamoto et al*., 2002; *Hillaire-Marcel et al*., 2004]. In general, sea-ice formation in the surface layer produces salty but isotopically light ($^{18}O$-depleted) brines, which sink in the water column and mix with subsurface waters. Conversely, the surface layer is provided with low-salinity, $^{18}O$-enriched water as a result of melting sea-ice [e.g., *Hillaire-Marcel and de Vernal*, 2008]. Isotopic excursions recorded in *Nps* from Arctic Ocean sediments were used to infer variations in sea-ice growth during Heinrich events [*Hillaire-Marcel and de Vernal*, 2008]. For the Okhotsk Sea, a mean $\delta^{18}O_{sw}$ deviation of $0.36 \pm 0.02$‰ to what would be expected from the salinity-$\delta^{18}O_{sw}$ relationship of *Yamamoto et al*. [2001] was found and ascribed to the influence of brines [*Yamamoto et al*., 2002]. Hence, our $\delta^{18}O_{ivc\text{-}sw}$ records might not unequivocally reflect past salinity changes. During winter, the northern part of the western Bering Sea is covered with sea-ice [*Niebauer et al*., 1999; *Zhang et al*., 2010], which might result in a stronger impact of brine rejection/sea-ice melt on the $\delta^{18}O_{ivc\text{-}sw}$ records toward our northern Bering Sea sites.

### 3.6. Biogenic Opal and $CaCO_3$

[18] Biogenic opal was measured on freeze-dried bulk sediment samples (20 mg) via molybdate-blue spectrophotometry [*Müller and Schneider*, 1993], and concentrations were calculated after *DeMaster* [1981] with a reproducibility of 1–2 wt %. Total carbon (TC) and total organic carbon (TOC) concentrations were determined using a Carlo Erba CNS Analyzer (model NA-1500), with TOC being measured on previously decalcified samples. Concentrations of $CaCO_3$ were indirectly calculated as the difference between TC and TOC, multiplied by 8.333.

## 4. Results

### 4.1. Temperature Reconstructions

[19] Figure 3A shows our $T_{Mg/Ca}$ results for the last 20 kyr together with the $SST_{Uk'37}$ records from *Max et al*. [2012]. Reconstructed $T_{Mg/Ca}$ have a similar range in all cores of about 2° to 6°C. Core 12KL recorded the most pronounced amplitude variations and a $T_{Mg/Ca}$ maximum of ~9°C. Alkenone concentrations before 15 ka BP are below detection limit and afterward the records reflect successively higher $SST_{Uk'37}$ from the north to the south of ~3°C [*Max et al*., 2012]. No meridional gradients are found for $T_{Mg/Ca}$. Relative temperature changes in $SST_{Uk'37}$ and $T_{Mg/Ca}$ consistently show a warming from H1 into the B/A and a cooling from the B/A into the YD at all sites (Figure 3A). The deglacial $SST_{Uk'37}$ evolution almost parallels the thermal evolution registered in the NGRIP ice core from Greenland, whereas the $T_{Mg/Ca}$ evolution does not. Most notably, $T_{Mg/Ca}$ and $SST_{Uk'37}$ records in part show different trends. All cores show $T_{Mg/Ca}$ values of ~3–4°C during the H1 cold phase, but only at Site 12KL a significant cooling of ~3°C is recorded with respect to the Last Glacial Maximum (LGM) (Figure 3A). At the end of H1 within only 1–2 kyr, $T_{Mg/Ca}$ increase by 2–4°C to maxima of ~5–6°C at all sites, but to ~9°C at Site 12KL. $SST_{Uk'37}$ also increase by 2–6°C to maxima of 6–8°C [*Max et al*., 2012]. While Bering Sea cores 85KL and 101KL recorded almost similar $T_{Mg/Ca}$ and $SST_{Uk'37}$ until the PB, cores 114-3 and 77KL show $\Delta T$ values of ~2–3°C during the B/A (Figure 4). Notably, core 12KL features negative $\Delta T$ values that are minimal (-6°C) at the onset of the B/A and subsequently increasing. Following the B/A, cores 114-3, 12KL, and 77KL recorded a $T_{Mg/Ca}$ cooling to minima of ~3–4°C recorded during the YD. Core 85KL still exhibits a strong Mg/Ca variability, but on average decreasing values since the B/A. $SST_{Uk'37}$ also decrease by 2–5°C into the YD [*Max et al*., 2012]. During the YD, $\Delta T$ is reduced to about +2°C at sites 114-3 and 77KL, to 0°C at Site 85KL, and it again becomes negative (-2°C) at Site 12KL (Figure 3A). At Site 12KL, a ~2°C warming from the YD into the PB is recorded with a pronounced $T_{Mg/Ca}$ maximum of ~6°C (~11.5 ka BP), whereas Bering Sea core 77KL shows $T_{Mg/Ca}$ of ~4°C, and Okhotsk Sea core 114-3 does not show significantly increased $T_{Mg/Ca}$. The PB is subject to or followed by a 1–2°C cooling to $T_{Mg/Ca}$ of ~3–4°C at all sites, which remain almost constant afterward. $SST_{Uk'37}$ increase by up to 5°C subsequent to the YD and culminate in maxima of 9–10°C between 11 and 9 ka BP [*Max et al*., 2012]. The early Holocene $SST_{Uk'37}$ maximum and the summer insolation maximum occur simultaneously (Figure 3A). Consequently, both temperature proxies significantly diverge during or shortly after the PB until ~10 ka BP, with $\Delta T$ maxima of up to 6°C. Notably, $\Delta T$ at Site 12KL has become positive only since the PB. Holocene $T_{Mg/Ca}$ values are lower than those of the B/A and YD, but are comparable to H1 values. For the last 9 kyr, records from cores 114-3, 12KL, and 77KL point to a gradual ~2°C decrease in $SST_{Uk'37}$, which in core 114-3 is interrupted between 9 and 7 ka BP by a cooling to YD levels [*Max et al*., 2012]. Hence, the $\Delta T$ evolution during the middle to late Holocene overall follows the $SST_{Uk'37}$ signal and records a $\Delta T$ minimum between 9 and 7 ka BP in core 114-3 (Figure 3A).

### 4.2. Reconstruction of $\delta^{18}O_{ivc\text{-}sw}$

[20] Reconstructed $\delta^{18}O_{ivc\text{-}sw}$ values range between -1‰ and +1‰ during the last 20 kyr, with the most prominent variability also being recorded at Site 12KL (Figure 3B). Notably, Bering Sea core 85KL and Okhotsk Sea core

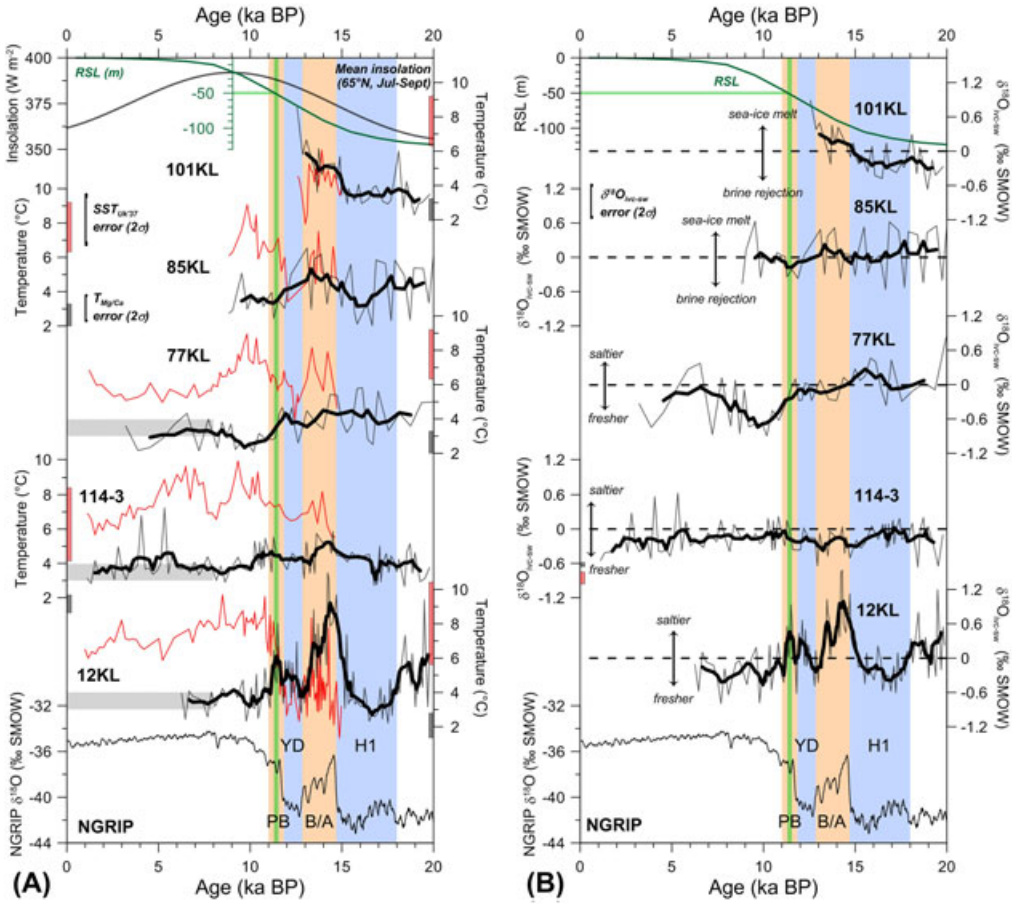


**Figure 3.** Temperature reconstructions (A) and ice volume–corrected seawater $\delta^{18}O$ estimates ($\delta^{18}O_{ivc\text{-}sw}$; B) over the last 20 kyr from the Bering Sea (SO201-2-101KL, -85KL, -77KL), the subarctic NW Pacific off Kamchatka (SO201-2-12KL), and the southern Okhotsk Sea (LV29-114-3). The NGRIP ice core oxygen isotope record (*NGRIP members*, 2004; GICC05 time scale, *Rasmussen et al*., 2006) is for reference. Running five-point-averages (thick black lines) are given to smooth the records of $T_{Mg/Ca}$ and $\delta^{18}O_{ivc\text{-}sw}$, and the respective uncertainties are indicated. Relative sea level (RSL, green line) is from *Waelbroeck et al*. [2002] and the green vertical bar marks the interval when RSL reached the approximate sill depth of the Bering Strait (~50 m). Pale orange and pale blue shadings represent the B/A and PB, and H1 and YD, respectively. In (A), the $T_{Mg/Ca}$ records (light gray lines) are shown together with the alkenone-based $SST_{Uk'37}$ records (thin red lines) from *Max et al*. [2012], plotted on the same scale. Average middle to late Holocene (<8 ka BP) temperature estimates of 3–4°C are highlighted (gray vertical bars), while the modern photic zone (0–30 m) and subsurface (50–100 m) temperature ranges are represented by red and gray vertical bars, respectively, next to the temperature axes (based on WOA data) [*Locarnini et al*., 2010] (cf. Figure 2). Mean insolation for boreal summer (July-September) at 65°N (thick gray line) was calculated after *Laskar et al*. [2004]. In (B), trends toward heavier (lighter) $\delta^{18}O_{ivc\text{-}sw}$ signatures are equivalent to increasing (decreasing) local subsurface salinity. Toward the northern Bering Sea sites, the $\delta^{18}O_{ivc\text{-}sw}$ signal is assumed to be additionally influenced by $^{18}O$-enriched meltwater during sea-ice melt and $^{18}O$-depleted brines during sea-ice formation. Dashed lines indicate $\delta^{18}O_{ivc\text{-}sw} = 0‰$ SMOW. Red and gray vertical bars next to the $\delta^{18}O_{ivc\text{-}sw}$ axes mark the modern $\delta^{18}O_{sw}$ ranges for the photic zone (0–30 m) and subsurface (50–100 m), respectively, at Okhotsk Sea station MU'6 [*Yamamoto et al*., 2001]. Notably, all records are characterized by negative average $\delta^{18}O_{ivc\text{-}sw}$ values after the PB.

114-3 show average values of 0‰ and -0.2‰, respectively, with only low and insignificant amplitude variability. Overall, relative changes in $\delta^{18}O_{ivc\text{-}sw}$ are regionally different, and for the Bering Sea sites opposing trends with a maximum gradient of ~0.4‰ are observed. However, at each site, a general covariation between $\delta^{18}O_{ivc\text{-}sw}$ and $T_{Mg/Ca}$ is found. During 20–18 ka BP, cores 12KL and 77KL show on average positive values (0‰ to +0.4‰), whereas $\delta^{18}O_{ivc\text{-}sw}$ is negative at sites 114-3 and 101KL (-0.3‰ to 0‰). During H1, Site 12KL is marked by a $\delta^{18}O_{ivc\text{-}sw}$ minimum of about -0.4‰ (Figure 3B). A similar significant extreme during that time is not observed at any other site. However, on average, core 77KL features positive values of about +0.2‰ during H1, whereas sites 101KL and 114-3 show negative values around -0.2‰. The transition from H1 into the B/A in core 77KL is characterized by decreasing

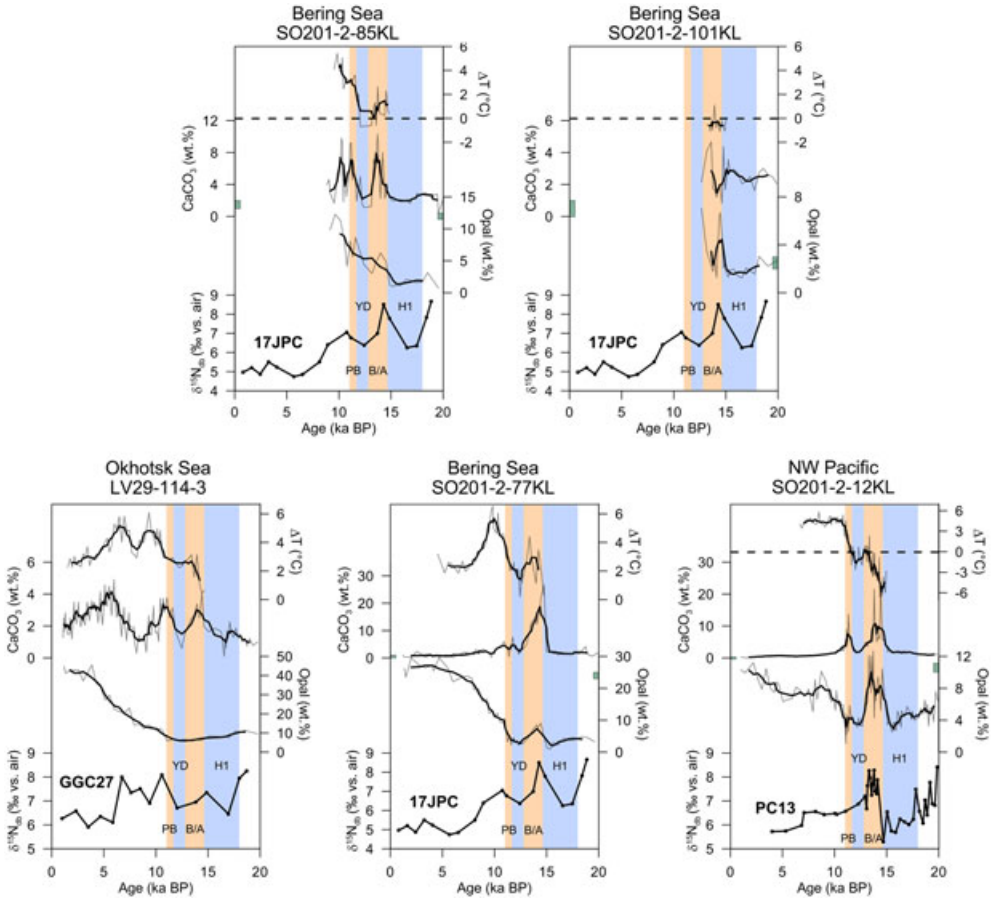


**Figure 4.** Temperature gradients ($\Delta T$) between $SST_{Uk'37}$ and $T_{Mg/Ca}$, and concentrations of $CaCO_3$ and biogenic opal for cores from the Bering Sea (SO201-2-77KL, -85KL, -101KL), the NW Pacific off Kamchatka (SO201-2-12KL), and the southern Okhotsk Sea (LV29-114-3). Data are smoothed by running five-point-averages (black lines). Dashed lines indicate $\Delta T = 0°C$. Green vertical bars next to the $CaCO_3$ and opal axes mark respective concentrations in surface sediments in the direct vicinity of the sediment core sites (stations SO201-2-11MUC, -76MUC, -83MUC, and -99MUC; Supplementary Information). For comparison, records of $\delta^{15}N_{db}$ from southern Okhotsk Sea core GGC27, southern Bering Sea core HLY02-02-17JPC, and open subarctic Pacific core PC13 are shown (data from *Brunelle et al*., 2007, 2010; cf. Figure 1). Pale orange and pale blue shadings represent the B/A and PB, and the H1 and YD, respectively.

$\delta^{18}O_{ivc\text{-}sw}$, while cores 12KL and 101KL show increasing values. At Site 12KL, this increase is reflected by a positive shift of about +1.4‰ occurring in less than 2 kyr (Figure 3B). During the B/A, Site 77KL shows negative values of about -0.2‰ prevailing until the onset of the PB. In contrast, positive values are recorded at sites 101KL (+0.3‰) and 12KL (+1‰), where the heaviest deglacial $\delta^{18}O_{ivc\text{-}sw}$ values are found. This core shows a decrease in $\delta^{18}O_{ivc\text{-}sw}$ during the B/A until a minimum of -0.2‰ at the onset of the YD, and a subsequent increase of 0.5‰ at 12.0 ka BP. Furthermore, core 12KL recorded a pronounced maximum of +0.5‰ during the PB (~11.5 ka BP), only found at this site, where it is subsequently followed by a sharp decrease to about -0.5‰ until ~10 ka BP (Figure 3B). Core 77KL also shows decreasing $\delta^{18}O_{ivc\text{-}sw}$ values since the onset of the PB until a minimum of -0.8‰ is reached at 10–9 ka BP. During the Holocene, $\delta^{18}O_{ivc\text{-}sw}$ values are negative at all sites varying between -0.1‰ and -0.8‰. Core 77KL from 9 to 6 ka BP shows a strong variability with on average increasing $\delta^{18}O_{ivc\text{-}sw}$ to about -0.1‰. Even lower values are subsequently preserved in this core until ~4 ka BP but affected by low temporal resolution.

## 5. Discussion

### 5.1. Deglacial Variability of Temperature and Salinity

[21] Our reconstructions show synchronous changes in $T_{Mg/Ca}$ and $\delta^{18}O_{ivc\text{-}sw}$ during the last deglaciation. These changes primarily reflect variations between "warm/salty" and "cold/fresh" subsurface waters. Core 114-3, at least during the H1 to B/A transition, appears to show the opposite relationship, but variability of $T_{Mg/Ca}$ and $\delta^{18}O_{ivc\text{-}sw}$ is low for this core and not significantly above measurement uncertainty. Hence, subsurface conditions at Site 114-3 might have remained fairly constant. Regional differences in the deglacial $\delta^{18}O_{ivc\text{-}sw}$ evolution are found, implying saltier subsurface conditions during the B/A and PB in the NW Pacific (Site 12KL), while the Bering Sea cores show opposing trends along the core transect. In contrast to sites 12KL and

101KL, sites 114-3 and 77KL indicate a freshening during the B/A. However, all cores indicate a freshening since the early Holocene. The deglacial $SST_{Uk'37}$ evolution is different from $T_{Mg/Ca}$ and characterized by warmings during the B/A and PB, coolings during the H1 and YD, and a subsequent cooling during the early Holocene. Hence, changes in $SST_{Uk'37}$ and N Atlantic climate occur quasi-synchronous [*Max et al*., 2012]. The developing gradients between surface and subsurface temperatures indicate changes in thermal MLS, which were different on a regional scale.

[22] Strong amplitude variations in $T_{Mg/Ca}$ and $\delta^{18}O_{ivc\text{-}sw}$ characterize Site 12KL, which might be explained oceanographically in the context of the major Bering Strait reopening. Today, the Alaskan Stream provides the NW Pacific and the Bering Sea with relatively fresh surface waters. Some authors speculated on reduced net inflow of Alaskan Stream waters into the Bering Sea when some of the Aleutian passes were closed due to lower glacial sea level [e.g., *Katsuki and Takahashi*, 2005; *Tanaka and Takahashi*, 2005]. The Bering Strait reopened between 12 and 11 ka BP [*Keigwin et al*., 2006]. Accordingly, the inflow of waters from the Alaskan Stream into the Bering Sea might have been reduced until the PB allowing for relatively enhanced accumulation of these water masses in the NW Pacific with respect to today. During H1 and the YD, this should consequently have resulted in more invigorated sea-ice formation and brine rejection (providing $^{18}O$-depleted water) in the northern Bering Sea, as well as in enhanced accumulation of cold/fresh Alaskan Stream waters in the NW Pacific. In contrast, during the B/A warm phase, sea-ice growth should have been reduced (providing less $^{18}O$-depleted brines), and relatively warmer and saltier waters should have accumulated in the NW Pacific. The weaker response at Site 12KL during the PB is then explained by higher sea level and an open Bering Strait, which resulted in stronger inflow of Alaskan Stream waters into the Bering Sea.

#### 5.1.1. Heinrich Stadial 1

[23] The above given considerations explain the presence of cold/fresh subsurface waters at Site 12KL during H1 (Figure 3). *Gebhardt et al*. [2008] also related drops in N Pacific salinity to North American river discharge and its subsequent transport via the Alaskan Current and Alaskan Stream rather than meltwater discharge from glacial ice sheets. This is in agreement with the absence of a Beringian Ice Sheet during the LGM [e.g., *Brigham-Grette et al*., 2001, 2003; *Karhu et al*., 2001]. Reduced inflow of Alaskan Stream waters into the Bering Sea can also account for the positive $\delta^{18}O_{ivc\text{-}sw}$ at Site 77KL, implying relatively increased subsurface salinity. At ODP Site 883D and at Site MD01-2416 in the NW Pacific, SSTs were higher than at our sites and characterized by three sharp increases of ~4–6°C [*Sarnthein et al*., 2006; *Gebhardt et al*., 2008]. These SST pulses are accompanied by locally increased salinity and were explained by short-term incursions of warm/salty Kuroshio waters. Warm $SST_{Uk'37}$ (20–24°C) of Kuroshio waters are confirmed for the last deglaciation [*Sawada and Handa*, 1998]. At Site GH02-1030, reconstructions from *Globigerina bulloides* show relatively saline conditions prevailing since the LGM, with a maximum at 15.5 ka BP and a subsequent decrease in both salinity and $T_{Mg/Ca}$ [*Sagawa and Ikehara*, 2008]. NE Pacific core MD02-2489 does also not show significantly higher SSTs during H1 [*Gebhardt et al*., 2008]. Hence, the northern Emperor Seamounts might provide a different oceanographic setting when compared to the far NW Pacific and the N Pacific marginal seas. Prior to ~15 ka BP, nondeterminable alkenone concentrations in our cores indicate restricted alkenone production by coccolithophores, most likely due to temperature limitation. Overall low marine productivity is supported by low biogenic opal concentrations. At the same time, light diatom-bound nitrogen isotope ratios ($\delta^{15}N_{db}$) in the subarctic Pacific realm [*Brunelle et al*., 2007, 2010] are indicative of a decrease in nitrate utilization in response to the enhanced supply of preformed nutrients from below and limited phytoplankton growth (Figure 4). Qualitative measurements of the sea-ice-related $IP_{25}$ proxy imply sea-ice influence at our sites during H1 and the YD, but absent or at least considerably reduced influence during the B/A and PB [*Max et al*., 2012]. *Gebhardt et al*. [2008] argued for pronounced phases of sea-ice formation in the subarctic N Pacific that induced vertical mixing during H1. Evidence for increased vertical mixing and/or intensified overturning during H1 and the YD comes from reduced ventilation ages [*Ohkushi et al*., 2004; *Sarnthein et al*., 2007; *Sagawa and Ikehara*, 2008; *Okazaki et al*., 2010], and is supported by climate modeling studies [e.g., *Okazaki et al*., 2010; *Chikamoto et al*., 2012; *Menviel et al*., 2012]. Moreover, benthic $\delta^{18}O$ excursions recorded in the northern Bering Sea imply that the Bering Sea was a proximate source of intermediate water during past stadial episodes [*Rella et al*., 2012]. Increased ventilation and the potential disappearance of the permanent halocline [*Menviel et al*., 2012] as a result of higher salinity is consistent with the reconstructions of *Sarnthein et al*. [2006] and *Sagawa and Ikehara* [2008]. It is presumably also supported by our study despite the regional differences in $\delta^{18}O_{ivc\text{-}sw}$, since results for sites 77KL and 114-3 indicate the presence of saltier subsurface waters (Figure 3B). The gradient in $\delta^{18}O_{ivc\text{-}sw}$ along our Bering Sea core transect rather reflects regional differences in sea-ice growth and according brine rejection. We propose that in the north, salty but $^{18}O$-depleted brines mixed with subsurface waters explaining the lower $\delta^{18}O_{ivc\text{-}sw}$ values with respect to Site 77KL.

#### 5.1.2. Bølling-Allerød

[24] Our records show maxima in $T_{Mg/Ca}$ at the onset or during the B/A and a subsequent cooling until the YD (Figure 3A). Considering sea–ice influence, more positive $\delta^{18}O_{ivc\text{-}sw}$ values until ~14.0 ka BP imply enhanced sea-ice melt or at least reduced sea-ice growth in the northern Bering Sea, whereas negative and decreasing $\delta^{18}O_{ivc\text{-}sw}$ values were recorded at sites 77KL and 114-3 indicating fresher subsurface conditions (Figure 3B). The recorded evolution of $T_{Mg/Ca}$ and $SST_{Uk'37}$ at our sites is congruent with results from the NW Pacific [*Sagawa and Ikehara*, 2008], the NE Pacific [*Kienast and McKay*, 2001; *Barron et al*., 2003; *Gebhardt et al*., 2008], the Bering Sea [*Caissie et al*., 2010], and the Okhotsk Sea [*Ternois et al*., 2000; *Harada et al*., 2006a; *Seki et al*., 2009]. The high $T_{Mg/Ca}$ of ~9°C at Site 12KL resemble conditions that today prevail in the Kuroshio Extension area (e.g., at WOA station 32070) [*Locarnini et al*., 2010] (cf. Figure 1), which, thus, argues for the northward expansion of the N Pacific gyre filled with Kuroshio waters as suggested by *Gebhardt et al*. [2008]. At the same time, increased N Pacific ventilation ages [*Adkins*

*and Boyle*, 1997; *Ahagon et al*., 2003; *Ohkushi et al*., 2004; *Sagawa and Ikehara*, 2008; *Okazaki et al*., 2010] imply reduced formation of deep/intermediate water masses. The presence of alkenones in all cores suggests that temperature limitation of coccolithophores was overcome. $\Delta T$ values of 0–1°C indicate weak thermal MLS at sites 85KL and 101KL due to relatively stronger sea-ice influence and still weak seasonal contrasts, which is supported by opal concentrations remaining low (<5 wt %; Figure 4). Sites 77KL and 114-3 also recorded only little higher opal concentrations. However, $T_{Mg/Ca}$ at these sites compare with those of sites 85KL and 101 KL, whereas $SST_{Uk'37}$ estimates are higher by 2–3°C (Figure 3A). This indicates more pronounced thermal MLS as a result of stronger seasonal contrasts. We propose that continuing deglacial sea-level rise resulted in enhanced net inflow of Alaskan Stream waters into the Bering Sea providing Site 77KL with relatively fresher subsurface waters, thereby explaining the decrease in $\delta^{18}O_{ivc\text{-}sw}$ from H1 into the YD (Figure 3B). Relatively fresher subsurface conditions at sites 77KL and 114-3 are consistent with surface freshening off Japan from 14.6 ka BP to 13.6 ka BP [*Sagawa and Ikehara*, 2008]. Previous studies conducted in the southern Bering and Okhotsk seas suggested surface freshening due to invigorated sea-ice melt from the observation of negative shifts in planktonic $\delta^{18}O$ and increasing abundances of the diatom species *Paralia sulcata* [*Gorbarenko et al*., 2004, 2005; *Seki et al*., 2004a]. In contrast, opal concentrations at Site 12KL of up to ~12 wt % are comparable with Holocene values and suggest significantly enhanced marine productivity. At the same time, heavy $\delta^{15}N_{db}$ were recorded in the southern Bering Sea and NW Pacific [*Brunelle et al*., 2010], implying enhanced nitrate utilization or even denitrification of nitrate as a result of stronger upper-ocean stratification (Figure 4). The negative $\Delta T$ values in core 12KL during the B/A could be related to a significantly warmer and deepened mixed layer during a prolonged summer season and reduced sea-ice influence. Consequently, for Site 12KL, we consider seasonal bias in $SST_{Uk'37}$ signal formation, and that during the B/A, $SST_{Uk'37}$ more likely represent early spring conditions. Coccolithophorid blooms that in the modern subarctic N Pacific occur already during spring are known [*Takahashi et al*., 2002], and for the Okhotsk Sea seasonal bias has been suggested before to explain similarly high LGM and Holocene $SST_{Uk'37}$ values [*Seki et al*., 2004b].

#### 5.1.3. The Younger Dryas and Preboreal

[25] The $T_{Mg/Ca}$ and $\delta^{18}O_{ivc\text{-}sw}$ evolution observed at sites 114-3, 12KL, and 77KL during the YD and PB (Figure 3) broadly matches that found in the NW Pacific [*Sarnthein et al*., 2004, 2006; *Gebhardt et al*., 2008; *Sagawa and Ikehara*, 2008], although our records show lower $\delta^{18}O_{ivc\text{-}sw}$ values. Lowered $SST_{Uk'37}$ during the YD are in agreement with the suggested southeastward expansion of the W Pacific Subarctic Gyre and the Bering Sea Gyre [*Kienast and McKay*, 2001], as well as with modeling results predicting a strengthened and eastward expanded Aleutian Low, which initiated better ventilation [*Mikolajewicz et al*., 1997]. This is also in agreement with reduced N Pacific ventilation ages [e.g., *Okazaki et al*., 2010]. At the same time, similar $T_{Mg/Ca}$ and $SST_{Uk'37}$ indicate weak but regionally different thermal MLS at our sites as a result of less developed seasonal contrasts. At sites 12KL, 77KL, and 114-3, $\Delta T$ values of ~2°C imply relatively stronger thermal MLS than at Site 85KL ($\Delta T = 0$°C), which recorded H1-like conditions (Figures 3 and 4). During the PB, $T_{Mg/Ca}$ and related $\delta^{18}O_{ivc\text{-}sw}$ values imply further subsurface cooling and freshening (77KL) and/or conditions still comparable to the YD (114-3). Concurrent increases in $SST_{Uk'37}$ argue for more pronounced thermal MLS, which is characterized by a deepening of the thermocline, extra cooling of sub-thermocline waters in hand with the formation of the dichothermal layer. We propose that at least our Bering Sea sites were now subject to increased inflow of relatively warmer Pacific surface waters through the Aleutian passes as a result of the reopening of the Bering Strait, and that this process fostered seasonal MLS by reducing the sea-ice growth.

#### 5.1.4. The Holocene

[26] Most notably for all our cores are the differently developing $T_{Mg/Ca}$ and $SST_{Uk'37}$ since the PB (Figure 3A), best explained by insolation changes affecting the surface ocean warming, reduced sea-ice, and increasing seasonal contrasts controlling the shape and position of the thermocline. Holocene $T_{Mg/Ca}$ remain either equal or stay lower than during H1 (Figure 3A). Our $T_{Mg/Ca}$, although being 1–2°C warmer, well reflect modern conditions, which is consistent with the NW Pacific studies [*Sarnthein et al*., 2004, 2006; *Gebhardt et al*., 2008; *Sagawa and Ikehara*, 2008]. Overall, $\delta^{18}O_{ivc\text{-}sw}$ values remain negative at all sites indicating relatively fresh subsurface conditions and almost stable seasonal contrasts. *Sarnthein et al*. [2004] reported on the long-term but stepwise decrease in subsurface salinity at Detroit Seamount during the early to middle Holocene, speculating that the modern salinity-driven stratification developed only since the Holocene. We can not confirm this stepwise salinity decline. However, our results point to a deglacial evolution of subsurface water mass characteristics developing into relatively fresh conditions along with enhanced thermal MLS (strong seasonal contrasts) since the early Holocene. Dominant control on the Holocene subarctic NW Pacific $SST_{Uk'37}$ evolution is attributed to Northern Hemisphere summer insolation [*Okumura et al*., 2009; *Hu et al*., 2010; *Max et al*., 2012]. In consequence, stronger seasonal contrasts developed as the result of a prolonged summer season and reduced sea-ice influence. Stronger winter mixing would have lead to the formation of the dichothermal layer. In this case, our high $\Delta T$ values of ~5–6°C would be explained by higher $SST_{Uk'37}$ due to stronger insolation, and by *Nps* recording gradually cooler subsurface temperatures due to the presence of the dichothermal layer. Accordingly, thermal MLS was consolidated and the seasonal halocline developed from sea-ice melt during summer. The largest difference between $T_{Mg/Ca}$ and $SST_{Uk'37}$ at ~10 ka BP coincides with the early Holocene thermal maximum, which in Alaska and northwest Canada occurred between 11 and 9 ka BP [*Kaufman et al*., 2004]. Recent model experiments indicate that besides insolation the reopening of the Bering Strait might have further affected this $SST_{Uk'37}$ maximum [*Okumura et al*., 2009; *Hu et al*., 2010]. Additionally, enhanced precipitation from the Westerlies and strengthened advection of cold/fresh waters from the Alaskan Stream might have contributed to the N Pacific cooling and freshening [*Sarnthein et al*., 2004].

### 5.2. Cause of Deglacial Stratification Changes and Impact on Atmospheric $CO_2$

[27] The deglacial $SST_{Uk'37}$ evolution recorded in the subarctic N Pacific realm appears to be related to and in-phase with the thermal evolution recorded in the N Atlantic realm, suggesting an atmospheric coupling [*Ternois et al*., 2000; *Kienast and McKay*, 2001; *Barron et al*., 2003; *Harada et al*., 2006a; *Seki et al*., 2009; *Caissie et al*., 2010; *Max et al*., 2012]. Several modeling studies investigated the sensitivity of the PMOC in response to perturbations of the AMOC on millennial time scales during the last deglaciation. All models predicted an enhanced PMOC at times of a weakened AMOC, whose strength was modulated by freshwater input into the Atlantic or by freshwater extraction from the Pacific [e.g., *Saenko et al*., 2004]. In the models, the weakened AMOC during H1 and the YD [e.g., *McManus et al*., 2004] results in the southward shift of the Intertropical Convergence Zone and in weakened Indian and Asian summer monsoons [*Zhang and Delworth*, 2005], which today maintain the salinity gradient between the Atlantic and Pacific [e.g., *Emile-Geay et al*., 2003]. Consequently, the antiphase models [e.g., *Saenko et al*., 2004] predicted a warming in the N Pacific due to the weakened AMOC, whereas the in-phase models [e.g., *Mikolajewicz et al*., 1997] suggested that atmospheric cooling by a strengthened Aleutian Low resulted in a PMOC. Interestingly, modeling results of *Chikamoto et al*. [2012] showed a cooling in the N Atlantic and in the NW Pacific, but ambiguous results for the NE Pacific. This was explained by a salinity increase in the N Pacific due to the weakened east Asian monsoon and changes in the oceanic transport of heat and salt. Both in-phase and antiphase models are supported by low ventilation ages in the N Pacific during H1 and the YD. Overall, our results support the studies of *Chikamoto et al*. [2012] and of *Menviel et al*. [2012], who discussed the effects of the removed halocline in the subarctic N Pacific. However, we cannot confirm strongly enhanced opal production, which was also predicted for H1 as a result of the established PMOC and the removal of the halocline [*Menviel et al*., 2012]. We rather attribute the low alkenone and opal concentrations observed at our sites to limitation of marine productivity by temperature and sea-ice. The notion of the removed halocline during H1 is supported by the high $\delta^{18}O_{ivc\text{-}sw}$ values recorded in NW Pacific cores MD01-2416 [*Sarnthein et al*., 2006; *Gebhardt et al*., 2008] and GH02-1030 [*Sagawa and Ikehara*, 2008]. During H1, our reconstructions indicate cold or decreasing surface and subsurface temperatures (atmospheric cooling), while our results for $\delta^{18}O_{ivc\text{-}sw}$ indicate a subsurface freshening at NW Pacific Site 12KL (strong Alaskan Stream). At the same time, saltier-than-today subsurface conditions are recorded at Bering Sea Site 77KL (weaker halocline), and increasing brine influence toward the north is assumed. The $T_{Mg/Ca}$ and $\delta^{18}O_{ivc\text{-}sw}$ recorded at our sites for the B/A and PB is explained by stronger seasonal MLS, which might be attributed to the reduced PMOC. Subsequent to the PB, the subarctic NW Pacific is subject to enhanced thermal MLS, which for the Bering Sea sites is possibly related to the opening of Bering Strait resulting in stronger inflow of N Pacific surface waters. Moreover, increased surface freshening during the Holocene potentially resulted from enhanced sea-ice melting during summer and enhanced precipitation.

[28] The deep N Pacific is suggested to have stored a greater portion of respired $CO_2$ during glacials than during interglacials [*Jaccard et al*., 2009]. During the last deglaciation, when the AMOC was strong, the respired carbon pool was removed from the deep sea, which is considered to have resulted in a deepening of the lysocline and an increase in atmospheric $CO_2$ [e.g., *Galbraith et al*., 2007]. Our records confirm increased $CaCO_3$ preservation and higher marine productivity during the B/A. Conversely, *Okazaki et al*. [2010] argued for enhanced N Pacific deep water formation during H1 (i.e., better ventilation when the AMOC was weak), and *Rella et al*. [2012] suggested that the Bering Sea was a proximate source for NPIW during that time. This is in agreement with the notion of a removed halocline, which would result in a rise in atmospheric $CO_2$ of 5 ppm [*Chikamoto et al*., 2012; *Menviel et al*., 2012]. Another aspect involves the efficiency of the biological pump. As recently summarized for the Pliocene, the subarctic N Pacific might have been responsible for higher atmospheric $CO_2$ in case of deep water formation resulting in a reduced ratio of regenerated-to-preformed nutrients in the ocean, thereby lowering the efficiency of the biological pump [*Studer et al*., 2012]. The $\delta^{15}N_{db}$ data of *Brunelle et al*. [2007, 2010] indeed argue for reduced nitrate utilization in the NW Pacific and its marginal seas during H1 and the YD (Figure 4). Since we reconstructed changes in thermal MLS, we can neither argue for nor against a change in the position and/or the strength of the permanent halocline. Nevertheless, our $\delta^{18}O_{ivc\text{-}sw}$ data show higher subsurface salinity in the southern Bering Sea (Site 77KL) during H1, but during the B/A in the NW Pacific (Site 12KL). This can at least be taken as supportive evidence for regional changes in subarctic N Pacific permanent halocline stability, which might therefore have contributed to the deglacial rise in atmospheric $CO_2$.

## 6. Conclusions

[29] We found regionally different changes in $T_{Mg/Ca}$ and $\delta^{18}O_{ivc\text{-}sw}$ in the subarctic NW Pacific as well as differences in alkenone- and Mg/Ca-based SST reconstructions. Our results indicate deglacial oceanographic changes in the mixed layer, which are most likely related to variations in Northern Hemisphere summer insolation and the strength of atmospheric pressure systems. Both factors control the extent of seasonal contrasts by driving changes in sea-ice formation, thereby altering seasonal MLS. From our results, we propose that seasonal contrasts and, hence, thermal MLS, although being regionally different, were reduced during H1 and the YD, but strong during the B/A. Our sites were characterized by low marine productivity, cold subsurface waters, and weak thermal MLS during the H1 and YD cold phases. This is attributed to an established PMOC and atmospheric cooling resulting in limited phytoplankton growth and enhanced sea-ice formation. Additional influence by increased advection of Alaskan Stream waters accumulating in the NW Pacific due to a closed Bering Strait is proposed. In contrast, warmer subsurface waters and regionally different temperature gradients were recorded during the B/A. At the same time, we found relatively increased $\delta^{18}O_{ivc\text{-}sw}$ in the NW Pacific (Site 12KL) and northern Bering Sea (Site 101KL), but reduced $\delta^{18}O_{ivc\text{-}sw}$ in the southern Okhotsk

and Bering seas (sites 114-3 and 77KL). This is explained by enhanced thermal MLS, accumulation of Alaskan Stream waters in the NW Pacific (at Site 12KL), as well as a stronger impact of brines on the $\delta^{18}O_{ivc\text{-}sw}$ signal in the northern Bering Sea. A decrease in $T_{Mg/Ca}$ and $\delta^{18}O_{ivc\text{-}sw}$ during the early Holocene along with high temperature gradients implies the only recent establishment of modern MLS in the subarctic NW Pacific and argues for subsurface oceanographic changes, which might be related to the reopening of the Bering Strait at 12–11 ka BP.

[30] **Acknowledgements.** This study was funded by the German Federal Ministry of Education and Research (BMBF; grant 03G0672A and B) and resulted from the joint German-Russian research project "KALMAR." Master and crew of R/V Sonne cruise SO201 Leg 2 are gratefully acknowledged for their professional support. E. Maier conducted additional opal measurements for core 77KL. We thank N. Gehre, L. Haxhiaj, B. Domeyer, and D. Poggemann for laboratory assistance and technical support, N. Khelifi for discussions, as well as two anonymous reviewers and the Editor for considerably improving the manuscript. The data are available via the PANGAEA Data Publisher for Earth & Environmental Science (http://doi.pangaea.de/10.1594/PANGAEA.786258).

## References

Adkins, J. F., and E. A. Boyle (1997), Changing atmospheric $\Delta^{14}C$ and the record of deep water paleoventilation ages, *Paleoceanography*, *12*(3), 337–344.

Ahagon, N., K. Ohkushi, M. Uchida, and T. Mishima (2003), Mid-depth circulation in the northwest Pacific during the last deglaciation: Evidence from foraminiferal radiocarbon ages, *Geophys. Res. Lett.*, *30*(21), 2097, doi:10.1029/2003GL018287.

Andersson, C., F. S. R. Pausata, E. Jansen, B. Risebrobakken, and R. J. Telford (2010), Holocene trends in the foraminifer record from the Norwegian Sea and the North Atlantic Ocean, *Clim. Past*, *6*(2), 179–193, doi:10.5194/cp-6-179-2010.

Barker, S., M. Greaves, and H. Elderfield (2003), A study of cleaning procedures used for foraminiferal Mg/Ca paleothermometry, *Geochem. Geophys. Geosyst.*, *4*(9), 8407, doi:10.1029/2003GC000559.

Barron, J. A., L. Heusser, T. Herbert, and M. Lyle (2003), High-resolution climatic evolution of coastal northern California during the past 16,000 years, *Paleoceanography*, *18*(1), 1020, doi:10.1029/2002PA000768.

Bauch, D., P. Schlosser, and R. G. Fairbanks (1995), Freshwater balance and the sources of deep and bottom waters in the Arctic Ocean inferred from the distribution of $H_2^{18}O$, *Prog. Oceanogr.*, *35*, 53–80.

Bauch, D., J. Carstens, and G. Wefer (1997), Oxygen isotope composition of living *Neogloboquadrina pachyderma* (sin.) in the Arctic Ocean, *Earth Planet. Sci. Lett.*, *146*, 47–58.

Bauch, D., H. Erlenkeuser, G. Winckler, G. Pavlova, and J. Thiede (2002), Carbon isotopes and habitat of polar planktic foraminifera in the Okhotsk Sea: The 'carbonate ion effect' under natural conditions, *Mar. Micropaleontol.*, *45*, 83–99, doi:10.1016/S0377-8398(02)00038-5.

Biebow, N., R. Kulinich, and B. Baranov (Eds.) (2003), Cruise Report: KOMEX (Kurile Okhotsk Sea Marine Experiment) RV Akademik M.A. Lavrentyev Cruise 29, Leg 1 and Leg 2, Vladivostok–Pusan–Okhostsk Sea–Pusan–Okhotsk Sea–Pusan–Vladivostok, May 25–August 05 2002, *GEOMAR Report*, *110*, 190, 176 pp.

Blockley, S. P. E., et al. (2012), Synchronisation of palaeoenvironmental records over the last 60,000 years, and an extended INTIMATE event stratigraphy to 48,000 b2k, *Quat. Sci. Rev.*, *36*, 2–10, doi:10.1016/j.quascirev.2011.09.017.

Brigham-Grette, J., D. M. Hopkins, V. F. Ivanov, E. B. Basilyan, S. L. Benson, P. A. Heiser, and V. S. Pushkar (2001), Last Interglacial (isotope stage 5) glacial and sea-level history of coastal Chukotka Peninsula and St. Lawrence Island, Western Beringia, *Quat. Sci. Rev.*, *20*, 419–436, doi:10.1029/2003GC000559.

Brigham-Grette, J., L. M. Gualtieri, O. Y. Glushkova, T. D. Hamilton, D. Mostoller, and A. Kotov (2003), Chlorine-36 and $^{14}C$ chronology support a limited Last Glacial Maximum across central Chukotka, northeastern Siberia, and no Beringian ice sheet, *Quat. Res.*, *59*, 386–398, doi:10.1016/S0033-5894(03)00058-9.

Brunelle, B. G., D. M. Sigman, M. S. Cook, L. D. Keigwin, G. H. Haug, B. Plessen, G. Schettler, and S. L. Jaccard (2007), Evidence from diatom-bound nitrogen isotopes for subarctic Pacific stratification during the last ice age and a link to North Pacific denitrification changes, *Paleoceanography*, *22*, PA1215, doi:10.1029/2005PA001205.

Brunelle, B. G., D. M. Sigman, S. L. Jaccard, L. D. Keigwin, B. Plessen, G. Schettler, M. S. Cook, and G. H. Haug (2010), Glacial/interglacial changes in nutrient supply and stratification in the western subarctic North Pacific since the penultimate glacial maximum, *Quat. Sci. Rev.*, *29*, 2579–2590, doi:10.1016/j.quascirev.2010.03.010.

Caissie, B. E., J. Brigham-Grette, K. T. Lawrence, T. D. Herbert, and M. S. Cook (2010), Last Glacial Maximum to Holocene sea surface conditions at Umnak Plateau, Bering Sea, as inferred from diatom, alkenone, and stable isotope records, *Paleoceanography*, *25*, PA1206, doi:10.1029/2008PA001671.

Chikamoto, M. O., L. Menviel, A. Abe-Ouchi, R. Ohgaito, A. Timmermann, Y. Okazaki, N. Harada, A. Oka, and A. Mouchet (2012), Variability in North Pacific intermediate and deep water ventilation during Heinrich events in two coupled climate models, *Deep-Sea Res. II*, *61-64*, 114–126, doi:10.1016/j.dsr2.2011.12.002.

DeMaster, D. (1981), The supply and accumulation of silica in the marine environment, *Geochim. Cosmochim. Acta*, *45*, 1715–1732.

Dullo, W.-C., B. Baranov, and C. van den Bogaard (Eds.) (2009), FS Sonne Fahrtbericht/Cruise Report SO201-2 KALMAR, Busan/Korea-Tomakomai/Japan, 30.08.-08.10.2009, *IFM-GEOMAR Report*, *35*, 233 pp.

Emile-Geay, J., M. A. Cane, N. Naik, R. Seager, A. C. Clement, and A. van Geen (2003), Warren revisited: Atmospheric freshwater fluxes and "Why is no deep water formed in the North Pacific", *J. Geophys. Res.*, *108*(C6), 3178, doi:10.1029/2001JC001058.

Galbraith, E. D., S. L. Jaccard, T. F. Pedersen, D. M. Sigman, G. H. Haug, M. Cook, J. R. Southon, and R. Francois (2007), Carbon dioxide release from the North Pacific abyss during the last deglaciation, *Nature*, *449*, 890–893, doi:10.1038/nature06227.

Gebhardt, H., M. Sarnthein, P. M. Grootes, T. Kiefer, H. Kuehn, F. Schmieder, and U. Röhl (2008), Paleonutrient and productivity records from the subarctic North Pacific for Pleistocene glacial terminations I to V, *Paleoceanography*, *23*, PA4212, doi:10.1029/2007PA001513.

Gorbarenko, S. A., J. R. Southon, L. D. Keigwin, M. V. Cherepanova, and I. G. Gvozdeva (2004), Late Pleistocene–Holocene oceanographic variability in the Okhotsk Sea: Geochemical, lithological and paleontological evidence, *Palaeogeogr. Palaeoclimatol. Palaeoecol.*, *209*, 281–301, doi:10.1016/j.palaeo.2004.02.013.

Gorbarenko, S. A., I. A. Basov, M. P. Chekhovskaya, J. Southon, T. A. Khusid, and A. V. Artemova (2005), Orbital and millenium scale environmental changes in the southern Bering Sea during the last glacial-Holocene: Geochemical and paleontological evidence, *Deep-Sea Res. II*, *52*, 2174–2185, doi:10.1016/j.dsr2.2005.08.005.

Grootes, P. M., M. Stuiver, J. W. C. White, S. Johnsen, and J. Jouzel (1993), Comparison of oxygen isotope records from the GISP2 and GRIP Greenland ice cores, *Nature*, *366*, 552–554.

Harada, N., K. H. Shin, A. Murata, M. Uchida, and T. Nakatani (2003), Characteristics of alkenones synthesized by a bloom of *Emiliania huxleyi* in the Bering Sea, *Geochim. Cosmochim. Acta*, *67*(8), 1507–1519, doi:10.1016/S0016-7037(02)01318-2.

Harada, N., N. Ahagon, T. Sakamoto, M. Uchida, M. Ikehara, and Y. Shibata (2006a), Rapid fluctuation of alkenone temperature in the southwestern Okhotsk Sea during the past 120 ky, *Global Planet. Change*, *53*, 29–46, doi:10.1016/j.gloplacha.2006.01.010.

Harada, N., M. Sato, A. Shiraishi, and M. C. Honda (2006b), Characteristics of alkenone distributions in suspended and sinking particles in the northwestern North Pacific, *Geochim. Cosmochim. Acta*, *70*, 2045–2062, doi:10.1016/j.gca.2006.01.024.

Haug, G. H., D. M. Sigman, R. Tiedemann, T. F. Pedersen, and M. Sarnthein (1999), Onset of permanent stratification in the subarctic Pacific Ocean, *Nature*, *401*, 779–782.

Haug, G. H., et al. (2005), North Pacific seasonality and the glaciation of North America 2.7 million years ago, *Nature*, *433*, 821–825, doi:10.1038/nature03332.

Hillaire-Marcel, C., A. de Vernal, L. Polyak, and D. Darby (2004), Size-dependent isotopic composition of planktic foraminifers from Chukchi Sea vs. NW Atlantic sediments—Implications for the Holocene paleoceanography of the western Arctic, *Quat. Sci. Rev.*, *23*, 245–260, doi:10.1016/j.quascirev.2003.08.006.

Hillaire-Marcel, C., and A. de Vernal (2008), Stable isotope clue to episodic sea ice formation in the glacial North Atlantic, *Earth Planet. Sci. Lett.*, *268*, 143–150, doi:10.1016/j.epsl.2008.01.012.

Hu, A., G. A. Meehl, B. L. Otto-Bliesner, C. Waelbroeck, W. Han, M.-F. Loutre, K. Lambeck, J. X. Mitrovica, and N. Rosenbloom (2010), Influence of Bering Strait flow and North Atlantic circulation on glacial sea-level changes, *Nat. Geosci.*, *3*, 118–121, doi:10.1038/ngeo729.

Jaccard, S. L., G. H. Haug, D. M. Sigman, T. F. Pedersen, H. R. Thierstein, and U. Röhl (2005), Glacial/interglacial changes in subarctic North Pacific stratification, *Science*, *308*, 1003-1006, doi:10.1126/science.1108696.

Jaccard, S. L., E. D. Galbraith, D. M. Sigman, G. H. Haug, R. Francois, T. F. Pedersen, P. Dulsky, and H. R. Thierstein (2009), Subarctic Pacific

evidence for a glacial deepening of the oceanic respired carbon pool, *Earth Planet. Sci. Lett.*, *277*, 156–165, doi:10.1016/j.epsl.2008.10.017.

Karhu, J. A., S. Tschudi, M. Saarnisto, P. Kubik, and C. Schlüchter (2001), Constraints for the latest glacial advance on Wrangel Island, Arctic Ocean, from rock surface exposure dating, *Global Planet. Change*, *31*, 447–451.

Katsuki, K., and K. Takahashi (2005), Diatoms as paleoenvironmental proxies for seasonal productivity, sea-ice and surface circulation in the Bering Sea during the late Quaternary, *Deep-Sea Res. II*, *52*, 2110–2130, doi:10.1016/j.dsr2.2005.07.001.

Katsumata, K., and I. Yasuda (2010), Estimates of non-tidal exchange transport between the Sea of Okhtosk and the North Pacific, *J. Oceanogr.*, *66*, 489–504, doi:10.1007/s10872-010-0041-9.

Kaufman, D. S., et al. (2004), Holocene thermal maximum in the western Arctic (0–180°W), *Quat. Sci. Rev.*, *23*, 529–560, doi:10.1016/j.quascirev.2003.09.007.

Keigwin, L. D., J. P. Donnelly, M. S. Cook, N. W. Driscoll, and J. Brigham-Grette (2006), Rapid sea-level rise and Holocene climate in the Chukchi Sea, *Geology*, *34*(10), 861–864, doi:10.1130/G22712.1.

Kiefer, T., M. Sarnthein, H. Erlenkeuser, P. M. Grootes, and A. P. Roberts (2001), North Pacific response to millennial-scale changes in ocean circulation over the last 60 kyr, *Paleoceanography*, *16*(2), 179–189, doi:10.1029/2003GC000559.

Kienast, S. S., and J. L. McKay (2001), Sea surface temperatures in the subarctic northeast Pacific reflect millennial-scale climate oscillations during the last 16 kyrs, *Geophys. Res. Lett.*, *28*(8), 1563–1566, doi:10.1029/2003GC000559.

Kohfeld, K. E., R. G. Fairbanks, S. L. Smith, and I. D. Walsh (1996), *Neogloboquadrina pachyderma* (sinistral coiling) as paleoceanographic tracers in polar oceans: Evidence from Northeast Water Polynya plankton tows, sediment traps, and surface sediments, *Paleoceanography*, *11*(6), 679–699, doi:10.1029/2003GC000559.

Kowalik, Z., J. L. Luick, and T. C. Royer (1994), On the dynamics of the Alaska Coastal Current, *Cont. Shelf Res.*, *14*(7/8), 831–845, doi:10.1029/2003GC000559.

Kozdon, R., A. Eisenhauer, M. Weinelt, M. Y. Meland, and D. Nürnberg (2009), Reassessing Mg/Ca temperature calibrations of *Neogloboquadrina pachyderma* (sinistral) using paired $\delta^{44/40}$Ca and Mg/Ca measurements, *Geochem. Geophys. Geosyst.*, *10*(3), Q03005, doi:10.1029/2008GC002169.

Krebs, U., and A. Timmermann (2007), Tropical air-sea interactions accelerate the recovery of the Atlatnic Meridional Overturning Circulation after a major shutdown, *J. Climate*, *20*, 4940–4956, doi:10.1175/jcli4296.1.

Kuroyanagi, A., and H. Kawahata (2004), Vertical distribution of living planktonic foraminifera in the seas around Japan, *Mar. Micropaleontol.*, *53*, 173–196, doi:10.1016/j.marmicro.2004.06.001.

Kuroyanagi, A., H. Kawahata, and H. Nishi (2012), Seasonal variation in the oxygen isotopic composition of different-sized planktonic foraminifer *Neogloboquadrina pachyderma* (sinistral) in the northwestern North Pacific and implications for reconstruction of the paleoenvironment, *Paleoceanography*, *26*, PA4215, doi:10.1029/2011PA002153.

Laskar, J., P. Robutel, F. Joutel, M. Gastineau, A. C. M. Correia, and B. Levrard (2004), A long-term numerical solution for the insolation quantities of the Earth, *Astron. Astrophys.*, *428*, 261–285, doi:10.1051/0004-6361:20041335.

Leduc, G., R. Schneider, J.-H. Kim, and G. Lohmann (2010), Holocene and Eemian sea surface temperature trends as revealed by alkenone and Mg/Ca paleothermometry, *Quat. Sci. Rev.*, *29*, 989–1004, doi:10.1016/j.quascirev.2010.01.004.

Locarnini, R. A., A. V. Mishonov, J. I. Antonov, T. P. Boyer, and H. E. Garcia (2010), World Ocean Atlas 2009, Volume 1: Temperature, in NOAA Atlas NESDIS 68, edited by S. Levitus, 184 pp, U.S. Government Printing Office, Washington, D.C.

Max, L., J.-R. Riethdorf, R. Tiedemann, M. Smirnova, L. Lembke-Jene, K. Fahl, D. Nürnberg, A. Matul, and G. Mollenhauer (2012), Sea surface temperature variability and sea-ice extent in the subarctic northwest Pacific during the past 15,000 years, *Paleoceanography*, *27*, PA3213, doi:10.1029/2012PA002292.

McManus, J. F., R. Francois, J.-M. Gherardi, L. D. Keigwin, and S. Brown-Leger (2004), Collapse and rapid resumption of Atlantic meridional circulation linked to deglacial climate changes, *Nature*, *428*, 834–837, doi:10.1038/nature02494.

Menviel, L., A. Timmermann, O. Elison Timm, A. Mouchet, A. Abe-Ouchi, M. O. Chikamoto, N. Harada, R. Ohgaito, and Y. Okazaki (2012), Removing the North Pacific halocline: Effects on global climate, ocean circulation and the carbon cycle, *Deep-Sea Res. II*, *61-64*, 106–113, doi:10.1016/j.dsr2.2011.03.005.

Mikolajewicz, U., T. J. Crowley, A. Schiller, and R. Voss (1997), Modelling teleconnections between the North Atlantic and North Pacific during the Younger Dryas, *Nature*, *387*, 384–387.

Miura, T., T. Suga, and K. Hanawa (2002), Winter mixed layer and formation of dichothermal water in the Bering Sea, *J. Oceanogr.*, *58*, 815–823, doi:10.1023/A:1022871112946.

Mohiuddin, M. M., A. Nishimura, and Y. Tanaka (2005), Seasonal succession, vertical distribution, and dissolution of planktonic foraminifera along the Subarctic Front: Implications for paleoceanographic reconstruction in the northwestern Pacific, *Mar. Micropaleontol.*, *55*, 129–156, doi:10.1016/j.marmicro.2005.02.007.

Müller, P., and R. Schneider (1993), An automated leaching method for the determination of opal in sediments and particulate matter, *Deep-Sea Res. I*, *40*, 425–444, doi:10.1029/2003GC000559.

Müller, P. J., G. Kirst, G. Ruhland, I. von Storch, and A. Rosell-Melé (1998), Calibration of the alkenone paleotemperature index $U^{K'}_{37}$ based on core-tops from the eastern South Atlantic and the global ocean (60°N–60°S), *Geochim. Cosmochim. Acta*, *62*(10), 1757–1772, doi:10.1029/2003GC000559.

Niebauer, H. J., N. A. Bond, L. P. Yakunin, and V. V. Plotnikov (1999), An update on the climatology and sea ice of the Bering Sea, in Dynamics of the Bering Sea, edited by T. R. Loughlin, and K. Ohtani, pp. 29–59, University of Alaska Sea Grant, doi:10.1029/2003GC000559.

North Greenland Ice Core Project members (2004), High-resolution record of northern hemisphere climate extending into the last interglacial period, *Nature*, *431*, 147–151, doi:10.1038/nature02805.

Ohkushi, K., M. Uchida, N. Ahagon, T. Mishima, and T. Kanematsu (2004), Glacial intermediate water ventilation in the northwestern Pacific based on AMS radiocarbon dating, *Nucl. Instrum. Methods Phys. Res. B*, *223-224*, 460–465, doi:10.1016/j.nimb.2004.04.087.

Ohtani, K., Y. Akiba, and A. Y. Takenouti (1972), Formation of western subarctic water in the Bering Sea, in Biological oceanography of the northern North Pacific Ocean, edited by A. Y. Takenouti, pp. 32–44, Idemitsu Shoten Publ. Co, doi:10.1029/2003GC000559.

Okazaki, Y., A. Timmermann, L. Menviel, N. Harada, A. Abe-Ouchi, M. O. Chikamoto, A. Mouchet, and H. Asahi (2010), Deepwater formation in the North Pacific during the last glacial termination, *Science*, *329*, 200–204, doi:10.1126/science.1190612.

Okumura, Y. M., C. Deser, A. Hu, A. Timmermann, and S.-P. Xie (2009), North Pacific climate response to freshwater forcing in the subarctic North Atlantic: Oceanic and atmospheric pathways, *J. Climate*, *22*, 1424–1445, doi:10.1175/2008jcli2511.1.

Rasmussen, S. O., et al. (2006), A new Greenland ice core chronology for the last glacial termination, *J. Geophys. Res.*, *111*, D06102, doi:10.1029/2005JD006079.

Regenberg, M., D. Nürnberg, S. Steph, J. Groeneveld, D. Garbe-Schönberg, R. Tiedemann, and W.-C. Dullo (2006), Assessing the effect of dissolution on planktonic foraminiferal Mg/Ca ratios: Evidence from Caribbean core tops, *Geochem. Geophys. Geosyst.*, *7*(7), Q07P15, doi:10.1029/2005GC001019.

Rella, S. F., R. Tada, K. Nagashima, M. Ikehara, T. Itaki, K. Ohkushi, T. Sakamoto, N. Harada, and M. Uchida (2012), Abrupt changes of intermediate water properties on the northeastern slope of the Bering Sea during the last glacial and deglacial period, *Paleoceanography*, *27*, PA3203, doi:10.1029/2011PA002205.

Saenko, O. A., A. Schmittner, and A. J. Weaver (2004), The Atlantic—Pacific seasaw, *J. Climate*, *17*(11), 2033–2038, doi:10.1175/1520-0442(2004)017.

Sagawa, T., and K. Ikehara (2008), Intermediate water ventilation change in the subarctic northwest Pacific during the last deglaciation, *Geophys. Res. Lett.*, *35*, L24702, doi:10.1029/2008GL035133.

Sarnthein, M., et al. (2001), Fundamental modes and abrupt changes in North Atlantic circulation and climate over the last 60 ky—Concepts, reconstruction and numerical modeling, in The northern North Atlantic: A changing environment, edited by P. Schäfer, W. Ritzrau, M. Schlüter, and J. Thiede, pp. 365–410, Springer, Berlin.

Sarnthein, M., H. Gebhardt, T. Kiefer, M. Kucera, M. Cook, and H. Erlenkeuser (2004), Mid Holocene origin of the sea-surface salinity low in the subarctic North Pacific, *Quat. Sci. Rev.*, *23*, 2089–2099, doi:10.1016/j.quascirev.2004.08.008.

Sarnthein, M., T. Kiefer, P. M. Grootes, H. Elderfield, and H. Erlenkeuser (2006), Warmings in the far northwestern Pacific promoted pre-Clovis immigration to America during Heinrich event 1, *Geology*, *34*(3), 141–144, doi:10.1130/G22200.1.

Sarnthein, M., P. M. Grootes, J. P. Kennett, and M.-J. Nadeau (2007), $^{14}$C reservoir ages show deglacial changes in ocean currents and carbon cycle, in Past and Future Changes of the Oceanic Meridional Overturning Circulation: Mechanisms and Impacts, edited by A. Schmittner, J. C. H. Chiang, and S. R. Hemming, pp. 175–196, AGU Monograph Series, 173, AGU, Washington, D.C.

Sawada, K., and N. Handa (1998), Variability of the path of the Kuroshio ocean current over the past 25,000 years, *Nature*, *392*, 592–595.

Schlitzer, R. (2011), Ocean Data View, http://odv.awi.de.

Schmittner, A., O. A. Saenko, and A. J. Weaver (2003), Coupling of the hemispheres in observations and simulations of glacial climate change, *Quat. Sci. Rev.*, *22*, 659–671, doi:10.1016/S0277-3791(02)00184-1.

Schmittner, A., E. D. Galbraith, S. W. Hostetler, T. F. Pedersen, and R. Zhang (2007), Large fluctuations of dissolved oxygen in the Indian and Pacific oceans during Dansgaard-Oeschger oscillations caused by variations of North Atlantic Deep Water subduction, *Paleoceanography*, *22*, PA3207, doi:10.1029/2006PA001384.

Seki, O., M. Ikehara, K. Kawamura, T. Nakatsuka, K. Ohnishi, M. Wakatsuchi, H. Narita, and T. Sakamoto (2004a), Reconstruction of paleoproductivity in the Sea of Okhotsk over the last 30 kyr, *Paleoceanography*, *19*, PA1016, doi:10.1029/2002PA000808.

Seki, O., K. Kawamura, M. Ikehara, T. Nakatsuka, and T. Oba (2004b), Variation of alkenone sea surface temperature in the Sea of Okhotsk over the last 85 kyrs, *Org. Geochem.*, *35*, 347–354, doi:10.1016/j.orggeochem.2003.10.011.

Seki, O., T. Nakatsuka, K. Kawamura, S.-I. Saitoh, and M. Wakatsuchi (2007), Time-series sediment trap record of alkenones from the western Sea of Okhotsk, *Mar. Chem.*, *104*, 253–265, doi:10.1016/j.marchem.2006.12.002.

Seki, O., T. Sakamoto, S. Sakai, S. Schouten, E. C. Hopmans, J. S. Sinninghe Damste, and R. D. Pancost (2009), Large changes in seasonal sea ice distribution and productivity in the Sea of Okhotsk during the deglaciations, *Geochem. Geophys. Geosyst.*, *10*(10), Q10007, doi:10.1029/2009GC002613.

Shackleton, N. J. (1974), Attainment of isotopic equilibrium between ocean water and the benthonic foraminifera genus *Uvigerina*: Isotopic changes in the ocean during the last glacial, *Colloques Internationaux du C.N.R.S. 219 – Les Méthodes Quantitatives D'étude des Variations du Climat au Cours du Pléistocène*, 203–209.

Sigman, D. M., and E. A. Boyle (2000), Glacial/interglacial variations in atmospheric carbon dioxide, *Nature*, *407*, 859–869.

Sigman, D. M., and G. H. Haug (2003), The biological pump in the past, in Treatise on Geochemistry, Vol. 6: The Oceans and Marine Geochemistry, edited by H. Elderfield, pp. 491–528, Elsevier-Pergamon.

Sigman, D. M., S. L. Jaccard, and G. H. Haug (2004), Polar ocean stratification in a cold climate, *Nature*, *428*, 59–63, doi:10.1038/nature02357.

Sigman, D. M., M. P. Hain, and G. H. Haug (2010), The polar ocean and glacial cycles in atmospheric $CO_2$ concentration, *Nature*, *466*, 47–55, doi:10.1038/nature09149.

Simstich, J., M. Sarnthein, and H. Erlenkeuser (2003), Paired $\delta^{18}O$ signals of *Neogloboquadrina pachyderma* (s) and *Turborotalia quinqueloba* show thermal stratification structure in Nordic Seas, *Mar. Micropaleontol.*, *48*, 107–125, doi:10.1016/S0377-8398(02)00165-2.

Stabeno, P. J., J. D. Schumacher, and K. Ohtani (1999), The physical oceanography of the Bering Sea, in Dynamics of the Bering Sea, edited by T. R. Loughlin, and K. Ohtani, pp. 1–28, University of Alaska Sea Grant.

Studer, A. S., A. Martínez-Garcia, S. L. Jaccard, F. E. Girault, D. M. Sigman, and G. H. Haug (2012), Enhanced stratification and seasonality in the subarctic Pacific upon Northern Hemisphere glaciation—New evidence from diatom-bound nitrogen isotopes, alkenones and archaeal tetraethers, *Earth Planet. Sci. Lett.*, *351-352*, 84–94, doi:10.1016/j.epsl.2012.07.029 .

Takahashi, K., N. Fujitani, and M. Yanada (2002), Long term monitoring of particle fluxes in the Bering Sea and the central subarctic Pacific Ocean, 1990-2000, *Prog. Oceanogr.*, *55*, 95–112, doi:10.1016/S0079-6611(02)00072-1.

Tanaka, S., and K. Takahashi (2005), Late Quaternary paleoceanographic changes in the Bering Sea and the western subarctic Pacific based on radiolarian assemblages, *Deep-Sea Res. II*, *52*, 2131–2149, doi:10.1016/j.dsr2.2005.07.002.

Ternois, Y., K. Kawamura, N. Ohkouchi, and L. Keigwin (2000), Alkenone sea surface temperature in the Okhotsk Sea for the last 15 kyr, *Geochem. J.*, *34*, 283–293, doi:10.1029/2003GC000559.

Tomczak, M., and J. S. Godfrey (1994), Regional oceanography: An introduction, 391 pp, Elsevier Science Ltd., Oxford.

Waelbroeck, C., L. Labeyrie, E. Michel, J. C. Duplessy, J. F. McMannus, K. Lambeck, E. Balbon, and M. Labracherie (2002), Sea-level and deep water temperature changes derived from benthic foraminifera isotopic records, *Quat. Sci. Rev.*, *21*, 295–305, doi:10.1016/S0277-3791(01)00101-9.

Warren, B. (1983), Why is no deepwater formed in the North Pacific?, *J. Mar. Res.*, *41*, 327–347, doi:10.1029/2003GC000559.

Weingartner, T. J., S. L. Danielson, and T. C. Royer (2005), Freshwater variability and predictability in the Alaska Coastal Current, *Deep-Sea Res. II*, *52*, 169–191, doi:10.1016/j.dsr2.2004.09.030.

Yamamoto, M., N. Tanaka, and S. Tsunogai (2001), Okhotsk Sea intermediate water formation deduced from oxygen isotope systematics, *J. Geophys. Res.*, *106*(C12), 31075–31084.

Yamamoto, M., S. Watanabe, S. Tsunogai, and M. Wakatsuchi (2002), Effects of sea ice formation and diapycnal mixing on Okhotsk Sea intermediate water clarified with oxygen isotopes, *Deep-Sea Res. I*, *49*, 1165–1174, doi:10.1016/S0967-0637(02)00032-8.

Yasuda, I. (1997), The origin of the North Pacific Intermediate Water, *J. Geophys. Res.*, *102*(C1), 893–909, doi:10.1029/2003GC000559.

You, Y. (2003), Implications of cabbeling on the formation and transformation mechanism of North Pacific Intermediate Water, *J. Geophys. Res.*, *108*(C5), 3134, doi:10.1029/2001JC001285.

Zhang, R., and T. L. Delworth (2005), Simulated tropical response to a substantial weakening of the Atlantic thermohaline circulation, *J. Climate*, *18*(12), 1853–1860, doi:10.1175/jcli3460.1.

Zhang, J., R. Woodgate, and R. Moritz (2010), Response to atmospheric and oceanic forcing in the Bering Sea, *J. Phys. Oceanogr.*, *40*(8), 1729–1747, doi:10.1175/2010jpo4323.1.